Chapter – 4

Mathematical Modeling

4.1 General

Due to the complexities of both the flow field and the scour mechanism, numerical modeling of the scour process around bridge piers remains a difficult research topic. Prediction of maximum scour depth around bridge pier is necessary for safe deign. Scour depth are determined by various methods, i.e. by use of empirical formula, physical model and theoretical approach. There have been few attempts to numerically model the flow field within a scour hole, much less couple such a hydrodynamic model with a sediment transport model to reproduce the growth of a scour hole. Commonly used equations and models are based on laboratory data. To get proper understanding of the flow structure around slender structure and its interaction with the channel bed needs more attention.

In this present chapter, an attempt has been made to study the flow behavior around slender structure that act as obstruction in flow path in rigid boundary open channel by mathematical modeling. The efficiency of channel section is determined analytically for rectangular and trapezoidal cross section with slender structure. The economic depth of flow and hydraulic radius is found for a given discharge with barrier in flow path. The energy of flow is determined with slender structure in rectangular channel section. The flow characteristics around circular and rectangular slender structure in flow path are studied extensively using ANSYS V 14.0 Fluent. The k-ϵ turbulence model is used to find the flow behavior around slender structure. The time averaged velocity component, turbulence kinetic energy are found at different vertical planes. The effect of multiple barriers in flow path is studied for rigid-boundary channel section. The effect of slender

structure embedded in sand bed of open channel is studied by using HEC-RAS keeping similarity with experimental study. The experimental results obtained in the present study are compared with the HEC- RAS results.

4.2 Influence of Slender Structure in Channel Section

The slender structures are those whose one direction dimension is much greater than other two directions. Bridge pier are construct in the river bed which is a slender structure and creates obstruction in flow path. Whenever, these structures are mounted on channel bed, the flow area reduces and the flow pattern changes which increase the velocities, kinetic energy and result in significant changes in flow parameters.

4.2.1 Efficiency of channel section with slender obstruction in flow path

An open channel is to be considered most efficient when it can passes maximum discharge for a given cross sectional area and bottom slope and resistance of flow in the side walls. If the energy loss due to resistance of flow from side walls and bottom slope remain constant along the reach of channel section, discharge is maximum when flow velocity is maximum. For a given value of slope and surface roughness, the flow will be maximum when hydraulic radius R is maximum. Hydraulic radius will be maximum if wetted perimeter of the channel is minimum.

The efficiency of channel section with rigid boundaries and slender barrier in flow path is solved analytically with elementary theory of hydraulics. In this study, it is assumed that there may be many numbers of similar type barriers in the flow path of the open channel section and these structures are slender in shape. It is also assumed that the slender structures are extended up to or above the free surface of the channel and rigidly mounted on rigid bed of the channel. The interference of side walls is neglected and side walls are rigid in nature i.e. no change of channel geometry with time occurs. The proposed solution is simple and can be used for design of efficient channel section with number of barriers in its flow path.

4.2.1.1 Rectangular channel section with slender barrier

A rectangular cross section channel is considered with n-numbers of barrier in its flow path as shown in Figure 4.1. The slender structures are placed in equal interval of the channel width. The width of the channel section is B and the depth of flow is y. It is assumed that the barriers are extended up to free surface and there is no interference of flow velocity. The discharge in upstream and downstream of the slender structure is same.

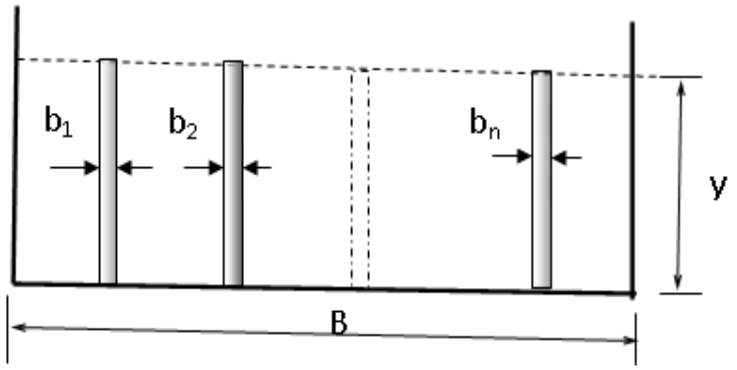

Figure 4.1: Cross section of rectangular shape open channel with n -number barriers

Let be Q the liquid discharge through the channel section when depth of flow is y. The hydraulic parameters without slender structures are as follows:

A is the wetted area, P is the wetted perimeter and hydraulic radius R = A/P.

The n numbers of slender barriers are mounted in the channel bed of width B at equal spacing. There are n-numbers of barriers whose projected width are $b_1, b_2 \ldots\ldots\ldots b_n$ as shown in Figure 4.1. As there are rigid barrier in the flow path, the effective width of the channel section will decrease. The hydraulic parameter at the section where the slender structures are mounted is A' is the wetted area, P' is the wetted perimeter and hydraulic radius R' = A'/P'

The effective width of channel section at the location of slender structure reduced to a value

$$B' = (B - b_1 - b_2 ..... - b_n) \quad 4.1$$

Wetted area of channel due to n numbers of obstruction present in channel cross section

$$A' = (B - b_1 - b_2 ..... - b_n) y \quad 4.2$$

If we assumed the width of each obstruction is same

$$\text{Let } b_1 = b_2 = ... = b_n = b \quad 4.3$$

Appling non dimensional obstruction factor for channel, Assume $\alpha = \frac{b}{B}$ dimensionless obstruction factor which produces $b = \alpha B$

Wetted area of channel is calculated in term of non-dimensional factor α, and then the equation 4.1 can be rewritten as

$$\text{Wetted area} \quad A' = B(1 - n\alpha) y \quad 4.4$$

$$\text{And} \quad B = \frac{A'}{(1 - n\alpha) y} \quad 4.5$$

Wetted perimeter of channel is calculated in term of non-dimensional factor (α)

$$P' = 2y + 2ny + (B - nb) \quad 4.6$$

Equation 4.6 can be re-written as

$$P' = 2y + 2ny + (1 - n\alpha) B \quad 4.7$$

$$P' = 2y + 2ny + (1 - n\alpha) \frac{A'}{(1 - n\alpha) y} \quad 4.8$$

$$P' = 2y + 2ny + \frac{A'}{y} \quad 4.9$$

For most efficient channel section, this wetted perimeter should be differentiated with respect to flow depth of channel section.

$$\frac{dP'}{dy} = 2 + 2n - \frac{A'}{y^2} \qquad 4.10$$

Condition for minimum wetted perimeter $\frac{dP'}{dy} = 0$ at the positions of the slender barriers in the flow path may be obtained in terms of depth of flow of water through the obstruction

$$y^2 = \frac{A'}{2(1+n)} \qquad 4.11$$

Putting equation 4.4 in the equation 4.11, yields the depth of flow in terms of non-dimensional obstruction factor and width of channel section and the channel section will be most efficient when the depth of flow is equal to

$$y = \frac{(1-n\alpha)B}{2(1+n)} \qquad 4.12$$

For more efficient channel section the bottom width must satisfy the following condition

$$B = \frac{2(1+n)y}{(1-n\alpha)} \qquad 4.13$$

$$\log B = \log 2 + \log(1+n) + \log y - \log(1-n\alpha) \qquad 4.14$$

Hydraulic radius at the section where the slender structures are mounted

$$R' = \frac{A'}{P'}$$

$$R' = \frac{B(1-n\alpha)y}{2y(1+n)+(1-n\alpha)B} \qquad 4.15$$

Putting the value of B for minimum wetted perimeter from equation 4.13 into the equation 4.15 yields.

$$R' = \frac{y}{2} \qquad 4.16$$

For a unit width of the channel section and barrier percentage 5% to 10% the economical depth of flow in the channel section is presented in Figure 4.2.

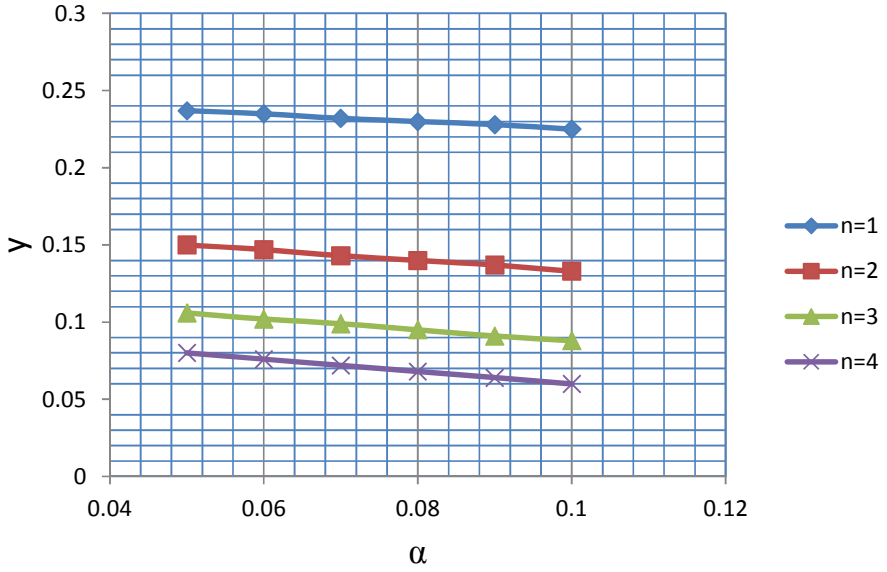

Figure 4.2: Economical Depth of flow with obstruction factor α in rectangular channel section

4.2.1.2 Trapezoidal channel section with slender barrier

Most efficient trapezoidal channel section with n-number slender barriers in flow path is derived from basic hydraulics. A channel section is considered to be most efficient when it can pass a maximum discharge for a given cross sectional area. For a trapezoidal channel section of bottom width B, top width T and side slopes θ_1 and θ_2 are considered for the analysis. There are n-numbers of barriers whose projected width are $b_1, b_2 \ldots\ldots\ldots\ldots b_n$ as shown in Figure 4.2 are mounted in the bottom width of the channel section.

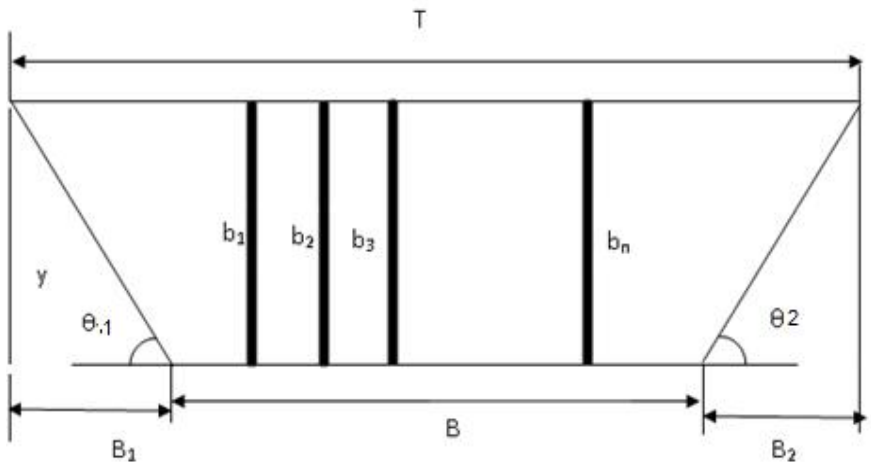

Figure 4.3: Cross section of Trapezoidal shape open channel with n -number of barriers

It is assumed that there is no pier structure in inclined side of the trapezoidal channel section. The slender structures are vertically mounted and the depth of flow is equal to the height of slender structure.

From Figure 4.3, one can determined the top width T and inclined side length in terms of side slope θ_1 and θ_2.

Top width of channel section may be expressed as

$$\begin{aligned} T &= B + B_1 + B_2 \\ T &= B + y(\cot\theta_1 + \cot\theta_2) \end{aligned} \qquad 4.17$$

Inclined length L_1 and L_2 can be written as

$$\begin{aligned} L_1 &= y \ \mathrm{cosec}\,\theta_1 \\ L_2 &= y \ \mathrm{cosec}\,\theta_2 \end{aligned} \qquad 4.18$$

Wetted perimeter, without slender barrier can be written as

$$\begin{aligned} P &= B + L_1 + L_2 \\ P &= B + y(\mathrm{cosec}\,\theta_1 + \mathrm{cosec}\,\theta_2) \end{aligned} \qquad 4.19$$

Wetted perimeter with n –number of obstruction can be written as

$$P' = L_1 + (2y + b_1) + (2y + b_2) + \ldots\ldots\ldots + (2y + b_n) + L_2$$

$$P' = L_1 + L_2 + 2ny + (b_1 + b_2 + ... + b_n) \quad 4.20$$

If we assume, the barriers are equal width of b and obstruction factor α

$$b = b_1 = b_2 = ... = b_n$$

$$\alpha = \frac{b}{B} = \frac{b_1}{B} = \frac{b_2}{B} ..... = \frac{b_n}{B} \quad 4.21$$

The wetted perimeter of equation 4.20 can be written as

$$P' = y(\text{cosec}\,\theta_1 + \text{cosec}\,\theta_2 + 2n) + n\alpha B \quad 4.22$$

Wetted area of the trapezoidal section without slender barrier

$$A = By + \frac{1}{2} y^2 (\cot\theta_1 + \cot\theta_2) \quad 4.23$$

The effective wetted area at the positions of n -numbers of equal barriers

$$A' = A - (b_1 y + b_2 y + ... + b_n y) \quad 4.24$$

If the barriers are equal width of dimension 'b' then wetted area can be written as

$$\begin{aligned} A' &= A - (nby) \\ A' &= A - n\alpha By \end{aligned} \quad 4.25$$

Equation 4.25 can be rewritten in terms of B and α

$$A' = (1 - n\alpha)By + \frac{y^2}{2}(\cot\theta_1 + \cot\theta_2) \quad 4.26$$

The bottom width of the channel section can be written as

$$B = \frac{A'}{(1 - n\alpha)y} - \frac{y}{2(1 - n\alpha)}(\cot\theta_1 + \cot\theta_2) \quad 4.27$$

Now Equation 4.22 can be rewritten as

$$P' = y(\text{cosec}\,\theta_1 + \text{cosec}\,\theta_2 + 2n) + n\alpha[\frac{A'}{(1 - n\alpha)y} - \frac{y}{2(1 - n\alpha)}(\cot\theta_1 + \cot\theta_2)] \quad 4.28$$

Assuming A' and side slope to be constant

$$\frac{\partial P'}{\partial y} = (\text{cosec}\,\theta_1 + \text{cosec}\,\theta_2 + 2n) - \frac{n\alpha A'}{(1 - n\alpha)y^2} - \frac{n\alpha}{2(1 - n\alpha)}(\cot\theta_1 + \cot\theta_2) \quad 4.29$$

To pass the maximum discharge through the channel section

$$\frac{\partial P'}{\partial y} = 0 \qquad 4.30$$

$$(\text{cosec}\,\theta_1 + \text{cosec}\,\theta_2 + 2n) - \frac{n\alpha A'}{(1-n\alpha)y^2} - \frac{n\alpha}{2(1-n\alpha)}(\cot\theta_1 + \cot\theta_2) = 0 \qquad 4.31$$

Putting the value of A' from equation 4.26 to equation 4.31 yields

$$\frac{n\alpha A'}{(1-n\alpha)y^2} = (\text{cosec}\,\theta_1 + \text{cosec}\,\theta_2 + 2n) - \frac{n\alpha}{2(1-n\alpha)}(\cot\theta_1 + \cot\theta_2)$$

$$\frac{n\alpha}{(1-n\alpha)y^2}\left[(1-n\alpha)By + \frac{y^2}{2}(\cot\theta_1 + \cot\theta_2)\right] = (\text{cosec}\,\theta_1 + \text{cosec}\,\theta_2 + 2n) - \frac{n\alpha}{2(1-n\alpha)}(\cot\theta_1 + \cot\theta_2)$$

4.32

$$\frac{y}{B} = \frac{n\alpha(1-n\alpha)}{(1-n\alpha)(\cos ec\,\theta_1 + \cos ec\,\theta_2 + 2n) - n\alpha(\cot\theta_1 + \cot\theta_2)} \qquad 4.33$$

Equation 4.33 is the required condition for a trapezoidal section with n-numbers of equal barrier in its flow path to be most economical.

The hydraulics radius R' can be expressed as $R' = \frac{A'}{P'}$

$$R' = \frac{(1-n\alpha)By + \frac{y^2}{2}(\cot\theta_1 + \cot\theta_2)}{y(\text{cosec}\,\theta_1 + \text{cosec}\,\theta_2 + 2n) + n\alpha B} \qquad 4.34$$

Putting the value of B from equation 4.33 in the expression of equation 4.34, the value of economical hydraulic radius in terms of depth of flow can be rewritten as

$$R' = \frac{(1-n\alpha)}{n\alpha}\frac{y}{2} \qquad 4.35$$

The economical depth of flow for trapezoidal channel section of unit width and equal side slope 1 (V): 2(H) is presented in Figure 4.4 for different obstruction factor ranges from 0.05 to 0.10.

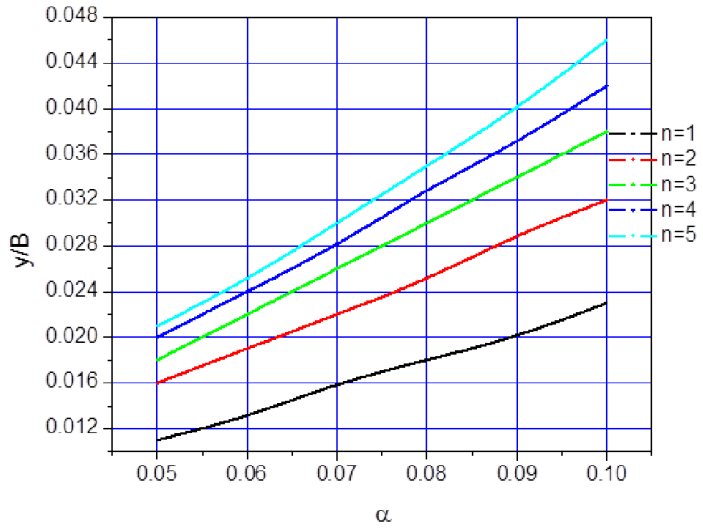

Figure 4.4: Economical depth for different obstruction factor

4.2.2 Energy of flow in channel section with slender obstruction in flow path

When, the water passes through the obstruction in flow path, the energy of flow in upstream section of the slender structure and downstream section changes. The total energy per unit weight of water is determined in upstream section where there are no obstruction and at the section of the barrier.

4.2.2.1 Rectangular channel section with slender obstruction

For a rectangular shape channel, the specific energy of flow at any cross section without any barrier in flow path is expressed by the

$$E = y + \frac{v^2}{2g} \tag{4.36}$$

Where, y is depth of flow and v is mean velocity at the section considered.

The energy of flow can be expressed in terms of $q = \frac{Q}{B}$, where Q is the discharge of the channel and q is the discharge per unit width of the channel, $A = By$ and $v = Q / A$. A is the wetted area.

The expression for specific energy in terms of q can be written as

$$E = y + \frac{q^2}{2gy^2} \tag{4.37}$$

The energy of flow will be minimum when $\frac{dE}{dy}=0$, this brings the condition of critical depth of flow where the flow energy is minimum. The critical depth of flow for a rectangular channel section is given by $y_c=\sqrt[3]{\frac{q^2}{g}}$ and corresponding energy of flow at critical condition is

$$E_c=\frac{3}{2}y_c \quad . \tag{4.38}$$

When, there are n-number of barriers in the flow path as shown in Figure 4.1, and the obstruction factor $\alpha=\frac{b}{B}$ the flow of energy is changed at the position of slender structure. Due to obstruction in flow path, the effective width of the channel section, depth of flow and wetted area will change.

Let the depth of flow at the barrier position is y' for same discharge Q.

Effective width at the position of the obstruction $B'=B-nb$

$$B'=B(1-n\alpha) \tag{4.39}$$

Wetted area $$A'=B(1-n\alpha)y' \tag{4.40}$$

The energy of flow at the position of slender structure

$$E'=y'+\frac{v'^2}{2g} \tag{4.41}$$

Where, $v'=\frac{Q}{A'}=\frac{Q}{B'y'}=\frac{q'}{y'}$ and $q'=\frac{Q}{b'}$

Then the energy at the section

$$E'=y'+\frac{q'^2}{2gy'^2} \tag{4.42}$$

q = flow per unit width without obstruction

and q' = flow per unit width with obstruction

$$\text{Now } \frac{q'}{q}=\frac{B}{B'}=\frac{B}{B(1-n\alpha)}=\frac{1}{1-n\alpha} \tag{4.43}$$

The relation between q and q' can be written as $q' = \frac{q}{1-n\alpha}$

The equation 4.42 can be rewritten as

$$E' = y' + \frac{q^2}{2gy'^2}\frac{1}{(1-n\alpha)^2} \tag{4.44}$$

For a given discharge, the condition for minimum specific energy at this section $\frac{dE'}{dy'} = 0$

The depth of flow corresponding to minimum energy of flow in the channel section is critical depth y_c' and it is obtained

Critical depth at this section

$$y_c' = \sqrt[3]{\frac{q^2}{g(1-n\alpha)^2}} \tag{4.45}$$

Now, the ratio of critical depth of flow at two sections for a given specific energy of flow (with slender structure and without slender structure) for maximum discharge in the channel section

$$\frac{y_c'^3}{y_c^3} = (1-n\alpha)^2 \tag{4.46}$$

The ratio of energy in the two sections in critical condition

$$E_c' = E_c\,(1-n\alpha)^{\frac{2}{3}} \tag{4.47}$$

The critical force at the section may be written as

$$F_c = \frac{1}{2}B'y_c'^2 + \frac{B'q'^2}{gy_c'} \tag{4.48}$$

The value of specific force at the section with obstruction is

$$F = B(1-n\alpha)\left[\frac{q^2}{g(1-n\alpha)^2}\right]^{\frac{2}{3}} \tag{4.49}$$

The variation of energy of flow for a unit discharge per unit width q=1 in the channel section is calculated for different number of barriers and obstruction factor 0.05 and presented in the Figure 4.5.

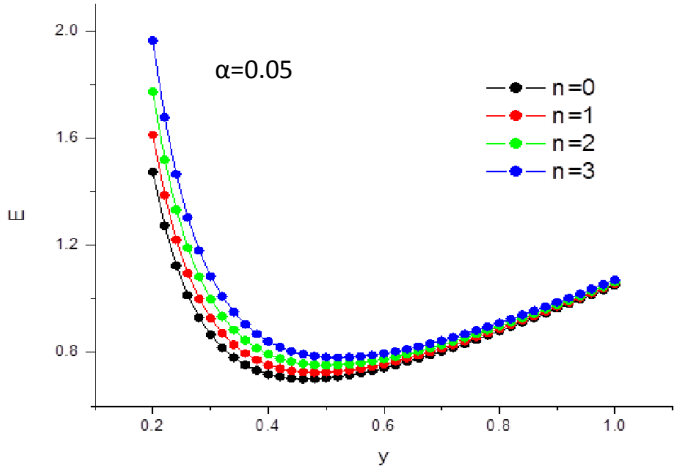

Figure 4.5: Energy of flow with depth of flow for α=0.05

It is observed from the Figure 4.5 and 4.6 that the energy of flow is lowest when there is no barrier in the section and the energy of flow increases with increasing the number of barriers in the channel section. When slender structure is placed in the section energy of flow increases and at downstream the loss of energy occurs.

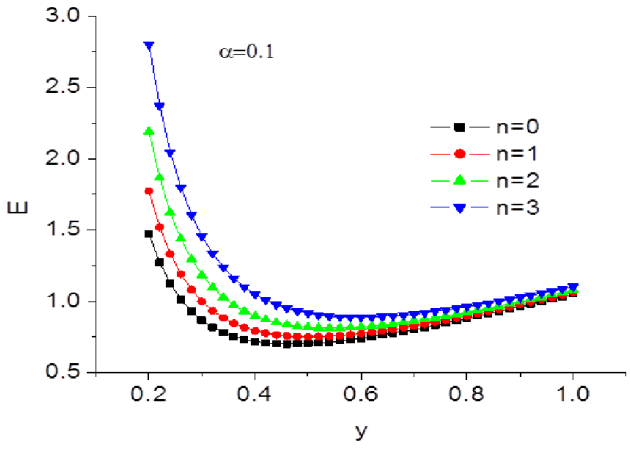

Figure 4.6: Energy of flow with depth of flow for α=0.1

34.3 Flow behavior around slender structure

The dynamics response of slender structure and fluid motions are governed by the combined actions of different external forces that rises from the fluid flow as well as by the inertia of the bodies themselves. The fluid structure interaction forces makes the system complex one. The analysis of the structure under fluid flow is a coupled problem where both motion of structure and fluid are affect each other. In fluid dynamics these forces can no longer be considered as acting at a single point or at discrete points of the system. As soon as fluid passes any solid surface vortex is formed and these vortices are moved and dissipate in the fluid medium. When an obstruction comes in between flow, flow separates moves around the object and flows downstream. At the point of contact, eddy currents or vortex are formed alternately on either side of the object. This creates a local increase in pressure and a local decrease in velocity on one side of the obstruction.

All the natural flows are governed by basic laws of physics. These include conservation of mass, momentum and energy. However in case of river dynamics (open channel flows) the major controlling equations are conservation of mass and momentum. The momentum equations for these types of flows are termed as Navior - Stokes equations. These equations are in the form of partial differential equations.

Governing equation

The momentum equation for the incompressible viscous fluid flow is

$$\frac{\partial \boldsymbol{u}}{\partial t} + (\boldsymbol{u}.\nabla)\boldsymbol{u} = -\frac{1}{\rho}\nabla p + \nu\nabla^2 \boldsymbol{u} \tag{4.50}$$

Where, **u** = Velocity Vector, ***p***= Pressure, **ρ**= Density of fluid, **ν**=Kinematic viscosity.

$$\frac{\partial u}{\partial t} + u\frac{\partial u}{dx} + v\frac{\partial u}{\partial y} + w\frac{\partial u}{\partial z} = -\frac{1}{\rho_f}\frac{\partial p}{\partial x} + \nu\left[\frac{\partial^2 u}{\partial x^2} + \frac{\partial^2 u}{\partial y^2} + \frac{\partial^2 u}{\partial z^2}\right]$$

$$\frac{\partial v}{\partial t} + u\frac{\partial v}{dx} + v\frac{\partial v}{\partial y} + w\frac{\partial v}{\partial z} = -\frac{1}{\rho_f}\frac{\partial p}{\partial y} + \nu\left[\frac{\partial^2 v}{\partial x^2} + \frac{\partial^2 v}{\partial y^2} + \frac{\partial^2 v}{\partial z^2}\right]$$

$$\frac{\partial w}{\partial t} + u\frac{\partial w}{dx} + v\frac{\partial w}{\partial y} + w\frac{\partial w}{\partial z} = -\frac{1}{\rho_f}\frac{\partial p}{\partial z} + \nu\left[\frac{\partial^2 w}{\partial x^2} + \frac{\partial^2 w}{\partial y^2} + \frac{\partial^2 w}{\partial z^2}\right] \tag{4.51}$$

Continuity equation

$$\nabla.\vec{u} = 0$$

$$\frac{\partial u}{\partial x} + \frac{\partial v}{\partial y} + \frac{\partial w}{\partial z} = 0 \tag{4.52}$$

In RANS these governing equations are averaged to give mean velocity values. In this way turbulent velocities are converted into two components, one is the average velocity and the other is its fluctuation. This fluctuation is modeled. While taking average of these equations, additional unknown terms are generated in these equations which are termed as Reynolds stresses. These stresses are solved with the help of turbulence models.
The governing equation in terms of Reynolds stresses are as follows

Momentum equations

$$x\text{ - direction: } u\frac{\partial u}{\partial x} + v\frac{\partial u}{\partial y} + w\frac{\partial u}{\partial z} = -\frac{1}{\rho}\frac{\partial p}{\partial x} + \frac{1}{\rho}\left(\frac{\partial \tau_{ii}}{\partial x} + \frac{\partial \tau_{ij}}{\partial y} + \frac{\partial \tau_{ik}}{\partial z}\right)$$

$$y\text{ - direction: } u\frac{\partial v}{\partial x} + v\frac{\partial v}{\partial y} + w\frac{\partial v}{\partial z} = -\frac{1}{\rho}\frac{\partial p}{\partial y} + \frac{1}{\rho}\left(\frac{\partial \tau_{ij}}{\partial x} + \frac{\partial \tau_{jj}}{\partial y} + \frac{\partial \tau_{jk}}{\partial z}\right)$$

$$z - direction: u\frac{\partial w}{\partial x} + v\frac{\partial w}{\partial y} + w\frac{\partial w}{\partial z} = -\frac{1}{\rho}\frac{\partial p}{\partial z} + \frac{1}{\rho}\left(\frac{\partial \tau_{ik}}{\partial x} + \frac{\partial \tau_{jk}}{\partial y} + \frac{\partial \tau_{kk}}{\partial z}\right) \tag{4.53}$$

Where *u, v, w* are velocity components in *x, y* and *z* directions, *p* is the pressure, ρ is density of fluid and τ_{ij} are shearing stresses (Reynolds stresses).

When, water passes through channel section or around slender structure, turbulent flow occurs. In turbulent flow, the instantaneous velocity (u, v, w) components can be represented by time averaged velocities and fluctuations (u', v', w') of time averaged velocity.

The continuity equation for fluctuating part

$$\frac{\partial u'}{\partial x} + \frac{\partial v'}{\partial y} + \frac{\partial w'}{\partial z} = 0 \tag{4.54}$$

Standard *k*- *ε* model

The turbulent kinetic energy *k* and its dissipation rate ***ε*** are determined using following transport equations.

$$u_i \frac{\partial k}{\partial x_i} = \frac{\partial}{\partial x_i}\left(\frac{v_t}{\sigma_k}\frac{\partial k}{\partial x_i}\right) - v_t\left(\frac{\partial u_i}{\partial x_j} + \frac{\partial u_j}{\partial x_i}\right)\frac{\partial u_i}{\partial x_j} - \varepsilon \quad (4.55)$$

$$u_i \frac{\partial \varepsilon}{\partial x_i} = \frac{\partial}{\partial x_i}\left(\frac{v_t}{\sigma_\varepsilon}\frac{\partial \varepsilon}{\partial x_i}\right) + c_{1_\varepsilon}\frac{\varepsilon}{k}P - c_{2_\varepsilon}\frac{\varepsilon^2}{k} \quad (4.56)$$

Where P= $v_t\left(\frac{\partial u_i}{\partial x_j} + \frac{\partial u_j}{\partial x_i}\right)\frac{\partial u_i}{\partial x_j}$

In these equations $\acute{c}_\mu$, σ_k , σ_ε , $c_{1\varepsilon}$, $c_{2\varepsilon}$ are empirical constants and their standard values are as follows.

$\acute{c}_\mu$ =0.09, σ_k =1.0, σ_ε =1.3, $c_{1\varepsilon}$ =1.44, $c_{2\varepsilon}$ =1.92

In the present study, the flow behavior around cylindrical and rectangular shape structure is found by solving the Naviers Stokes equation and K-ϵ model. For solution purpose standard software ANSYS 14.0 is used. The flow pattern and shear stresses on the pier structures are found by solving the same problem as dealt in the experimental study.

4.3.1 Flow behavior around cylindrical obstruction

The flow field around a circular cylinder mounted on channel bed is studied numerically. The flow pattern and its characteristics around various diameter of cylinder are modeled by using ANSYS Fluent. The analysis is performed for three different diameter of cylindrical slender structure for different velocity. One typical computational domain is shown in Figure 4.7.

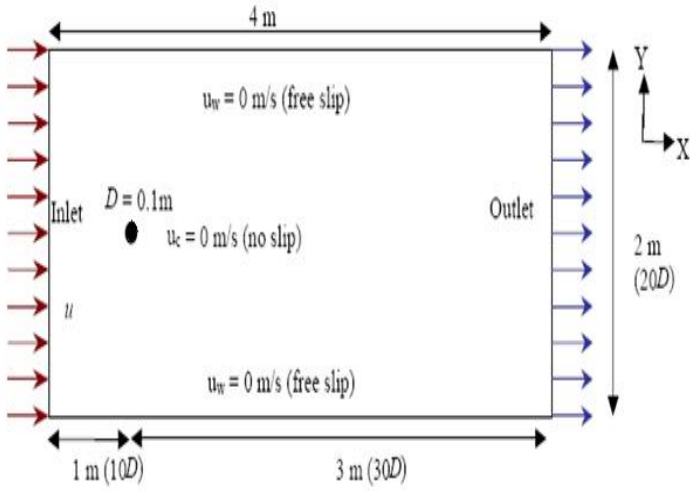

Plan of the model

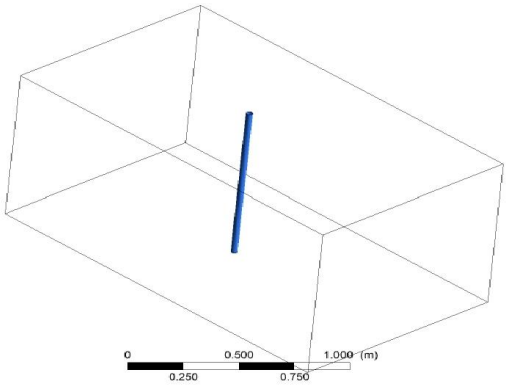

Figure 4.7: Cylindrical structure inside the computational domain

The velocity field, stream line and pressure variation near the slender structures are found and presented in the Figure 4.8 for different depth of flow and stream velocity.

The velocity field is found around a cylindrical diameter of D= 0.3 m for different free stream velocity of v=2, 3, 4 and 5m/s and presented in Figure 4.8. In the numerical model, the diameter of the pier is chosen as the same diameter which is used in the experiments. In the experiments, it was difficult to take many velocity data for plot the velocity field around slender structure.

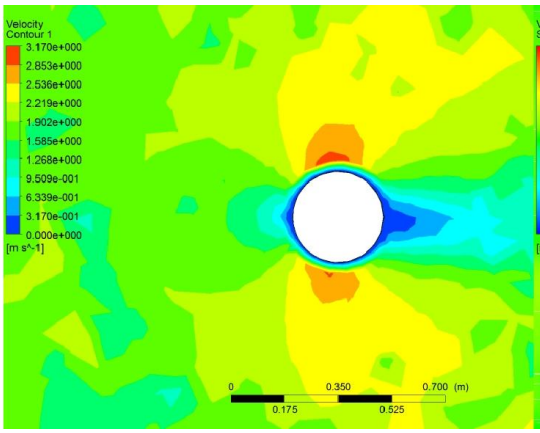

Velocity contour, v = 2 m/s

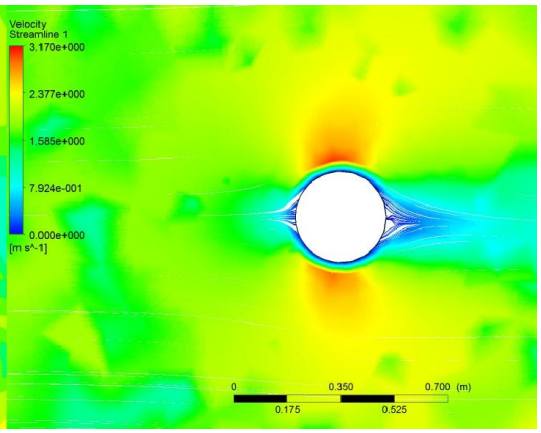

Velocity Streamline, v = 2 m/s

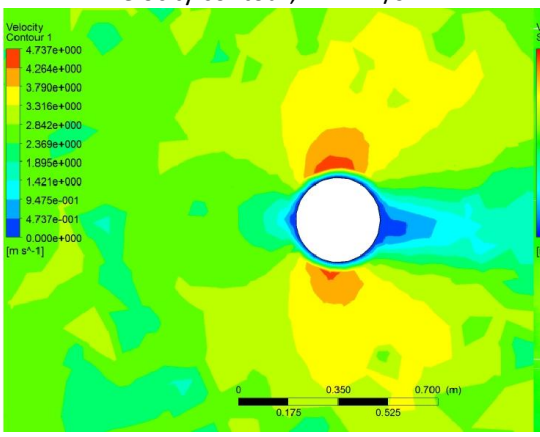

Velocity contour, v = 3 m/s

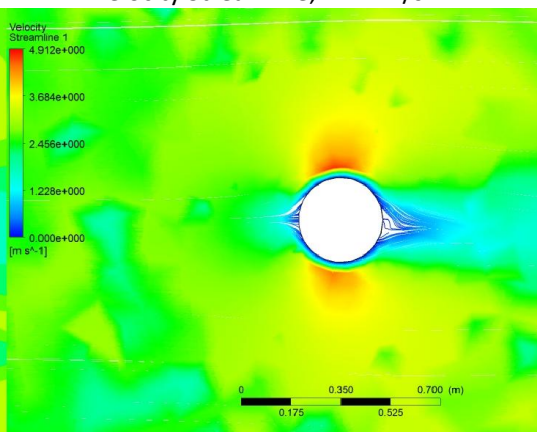

Velocity Streamline, v = 3 m/s

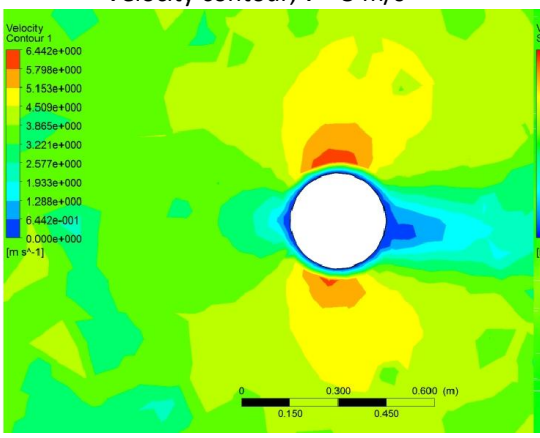

Velocity contour, v = 4 m/s

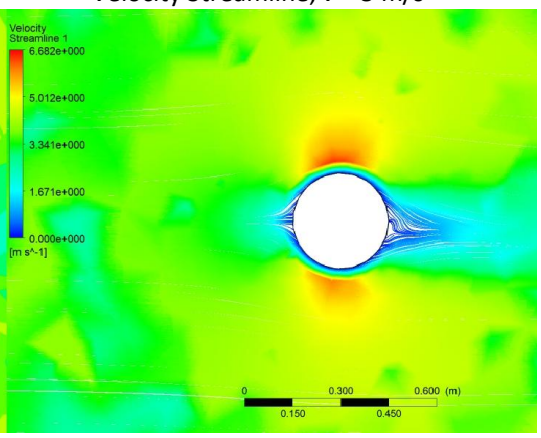

Velocity Streamline, v = 4 m/s

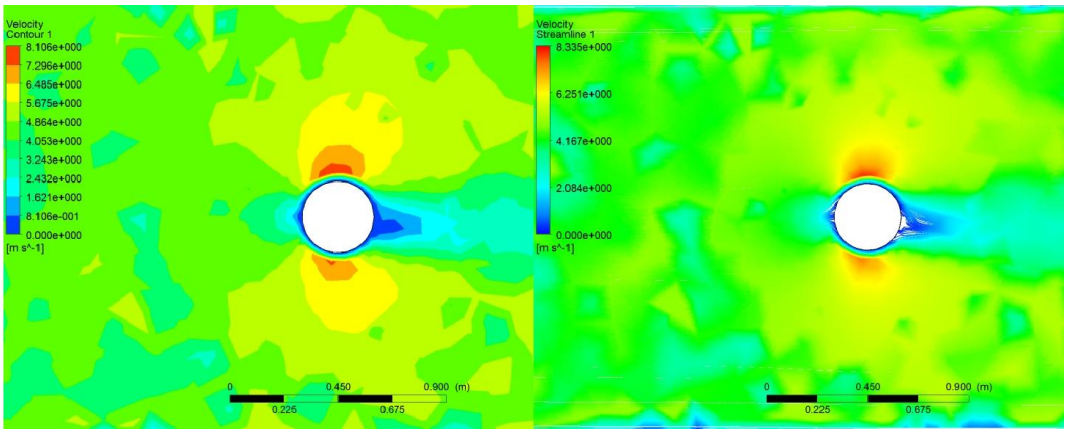

Velocity contour, v = 5 m/s Velocity Streamline, v = 5 m/s

Figure 4.8: Flow field around cylindrical pier at a plane 0.1m from bed level

In numerical analysis, the velocity vector and shape of stream line easily plotted. It is observed from Figure 4.8 that the flow pattern is changes with the velocity and vortex formation occurs at the downstream section.

The velocity contour, velocity vector, velocity streamline, total pressure contour and turbulent kinetic energy are found by numerical modeling. Three different diameter of pier was mounted on the rigid bed and a flow velocity passes through the piers. The diameter of piers were d= 0.1 m, 0.2m, and 0.3m and free stream velocity 2 m/s. The results are obtained in a plane at 0.1 m from bottom and presented for three different diameter of cylinder and presented in Figure 4.9.

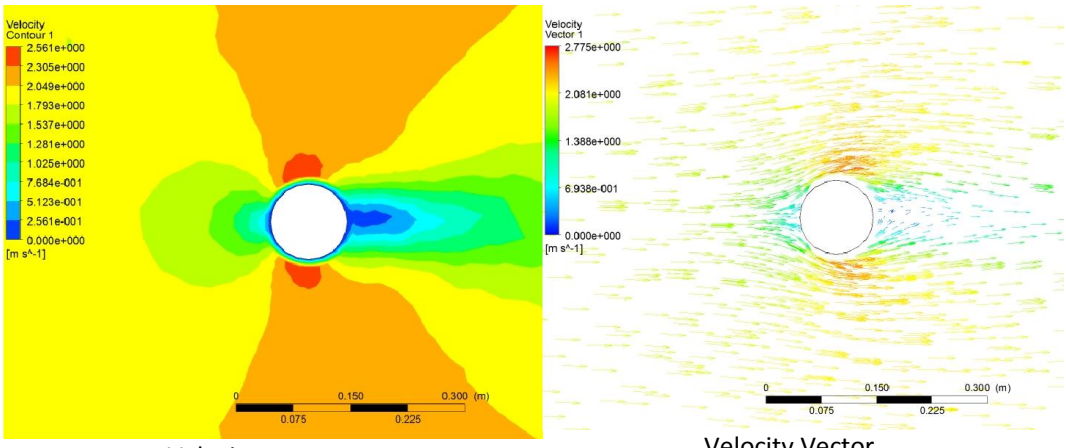

Velocity contour Velocity Vector

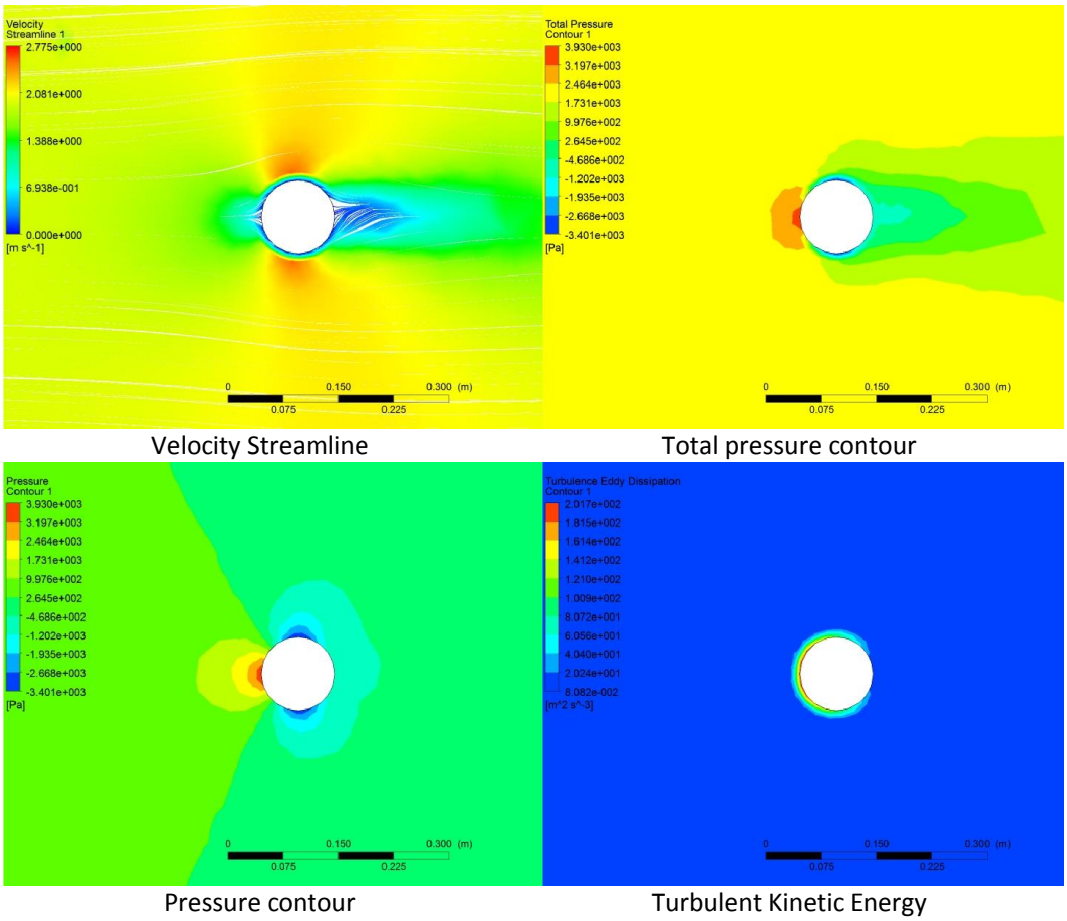

Velocity Streamline | Total pressure contour

Pressure contour | Turbulent Kinetic Energy

Figure 4.9: Flow filed around cylindrical structure of diameter 0.1 m

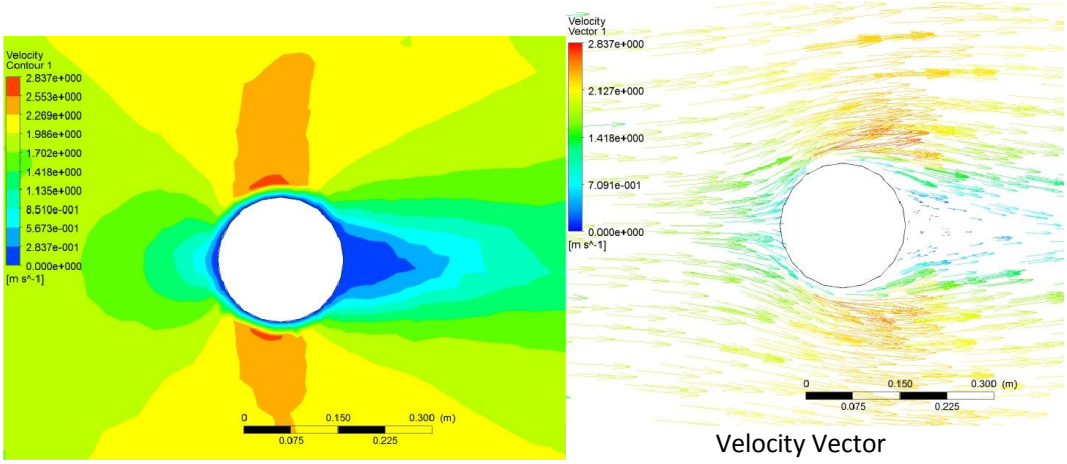

Velocity contour

Velocity Vector

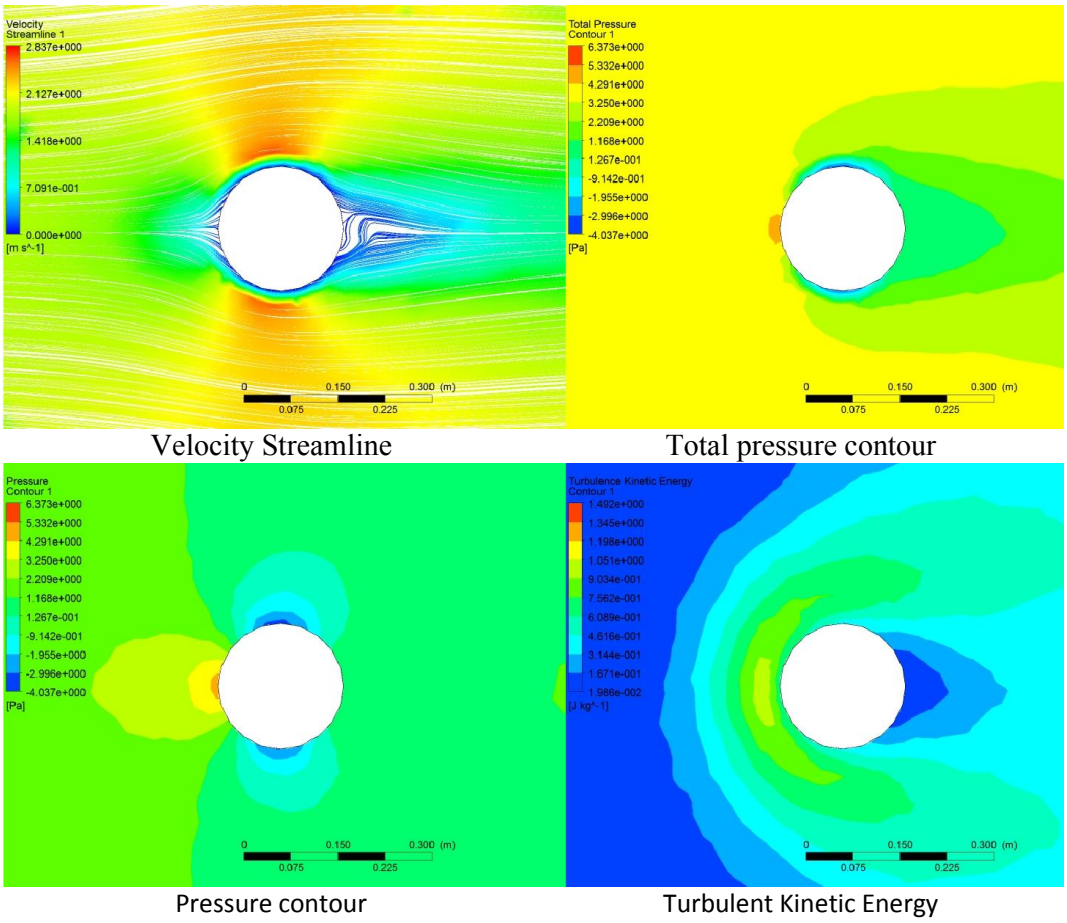

Figure 4.10: Flow filed around cylindrical structure of diameter 0.2 m

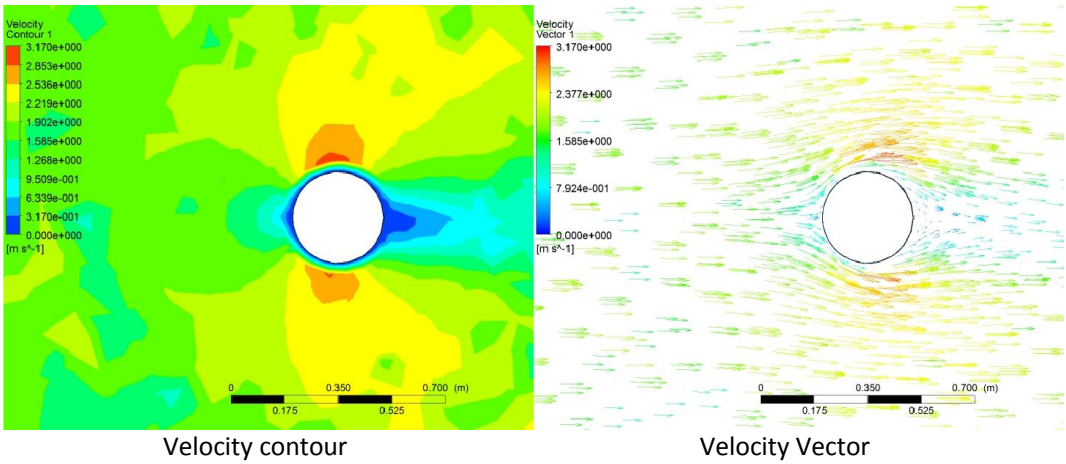

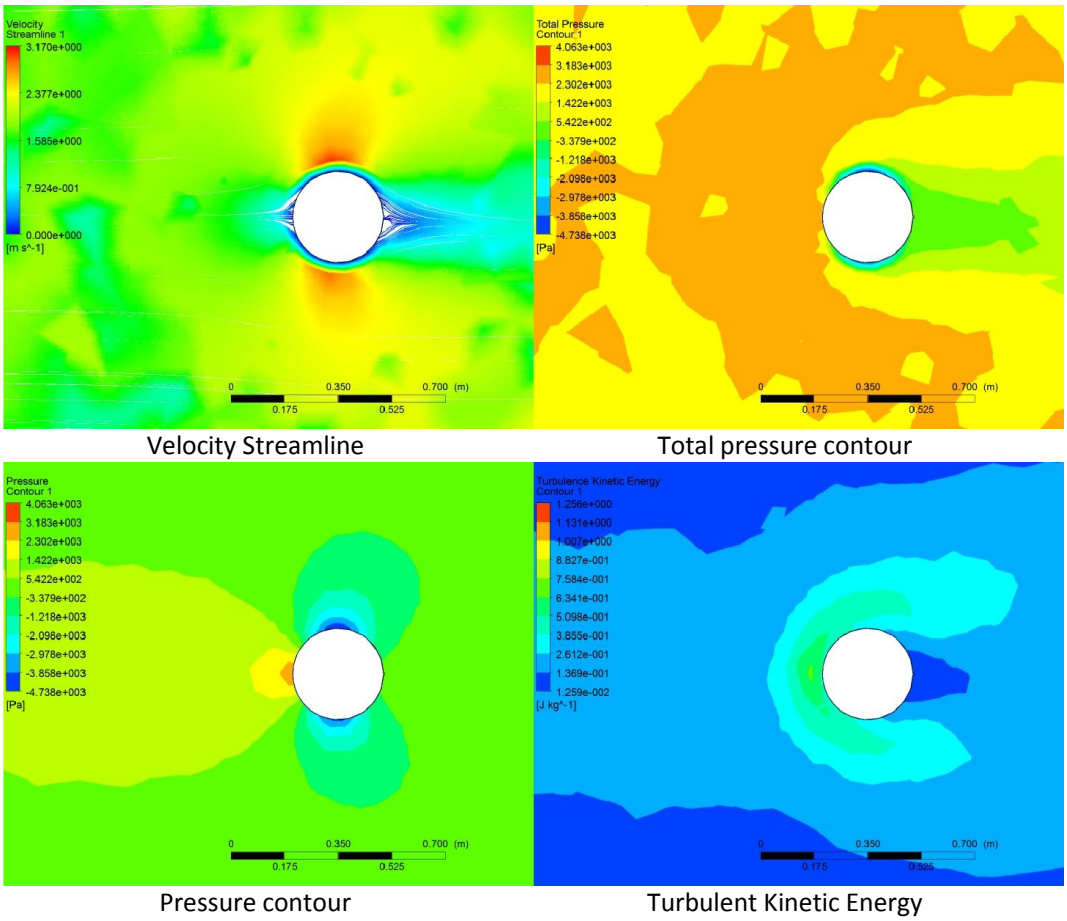

Figure 4.11: Flow filed around cylindrical structure of diameter 0.3 m

4.3.2 Flow characteristics around slender structure with multiple obstruction in flow path

The flow behavior around multiple obstructions in flow path is carried out. The slender structures are mounted vertically on the base of the computational domain. The spacing between piers is important parameter to change the flow pattern in the channel. The ratio r is defined as the spacing between piers to diameter of pier. The computational domain along with cylindrical piers is shown in the Figure 4.12.

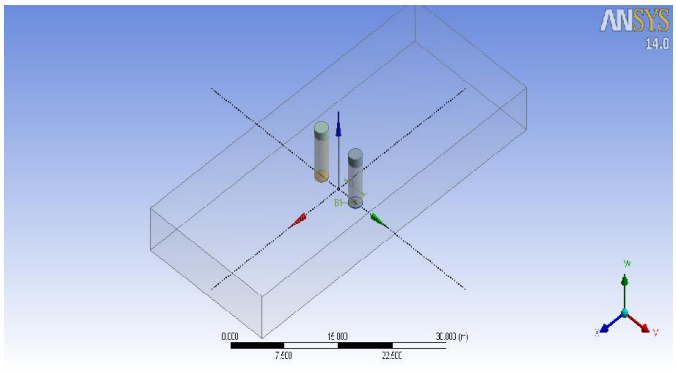

Figure 4.12 (a): Computational domain with two piers and r= 2.33

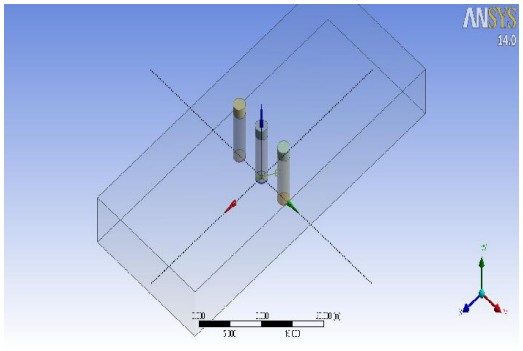

Figure 4.12 (b): Computational domain with three piers and r=1.5

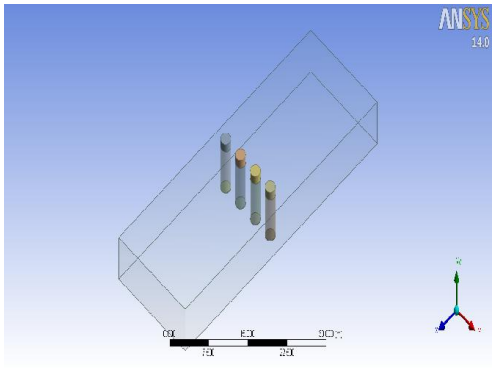

Figure 4.12 (c): Computational domain with four piers and r= 1

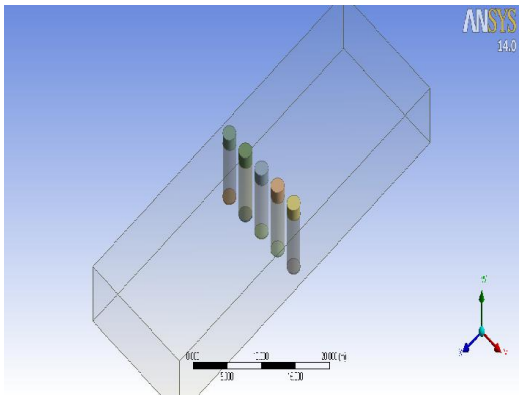

Figure 4.12 (d): Computational domain with five piers and r= 0.67

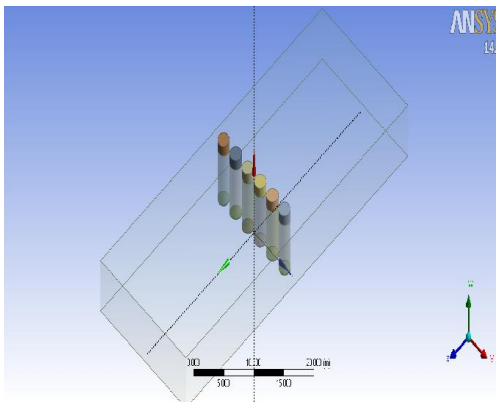

Figure 4.12 (e): Computational domain with six piers and r= 0.43

The r values are kept as r= 2.33, 1.5, 1.0, 0.67, 0.43 for the piers and a constant inlet flow velocity is passes through the cylindrical obstruction. In this section, the variation of velocity field, upstream and downstream pressure contour and kinetic energy of the flow is calculated and presented. The velocity contour is found or different cylinders and presented in Figure 4.13

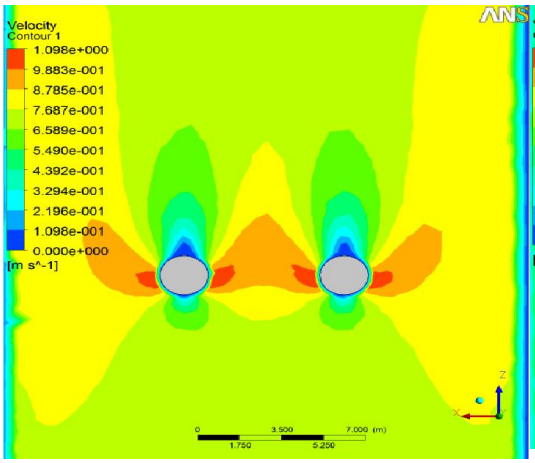

Figure 4.13 a: Velocity contour with two piers

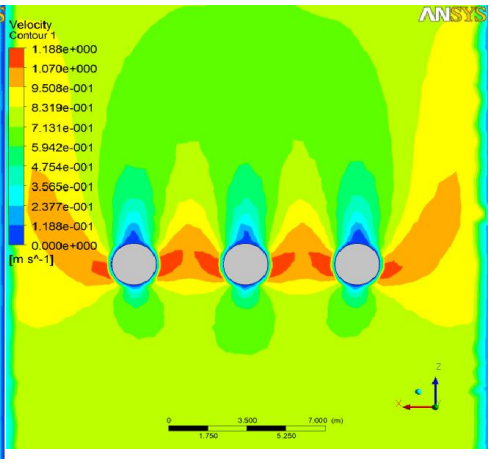

Figure 4.13b: Velocity contour with three piers

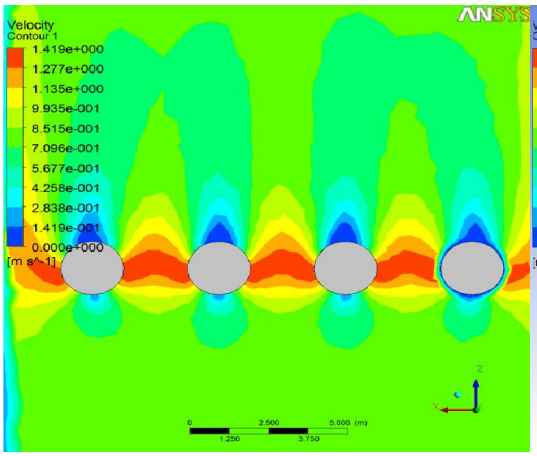

Figure 4.13c: Velocity contour with four piers

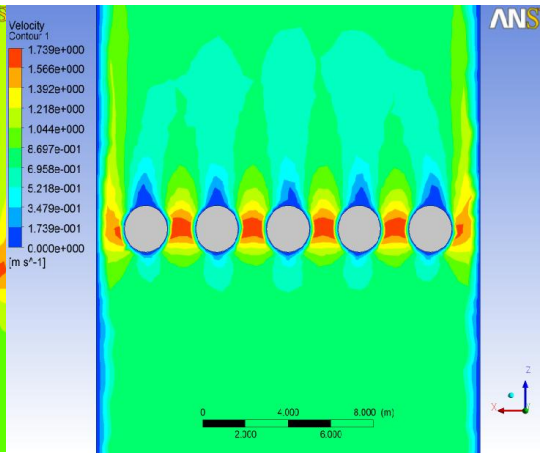

Figure 4.13d: Velocity contour with five piers

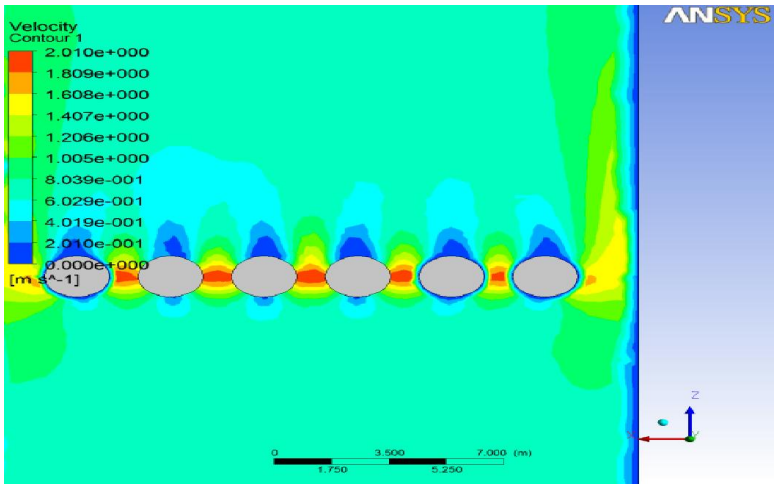

Figure 4.13e: Velocity contour with six piers

Figure 4.13: Velocity contour around multiple slender structures

It is observed from Figure 4.13 that the velocity field changes when the spacing between two piers are changing. When the r value is 2.33, there were no interfering of velocity field and on decreasing the r value, the interfering occurs in the flow field.

The variations of pressure field around the structures are shown in Figure 4.14 with multiple barriers. The pressure field is found for an inlet velocity 0.75m/s in the computational domain.

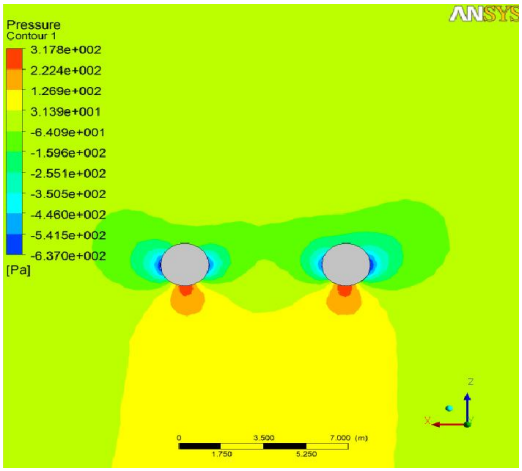

Figure 4.14a: Pressure contour with two piers

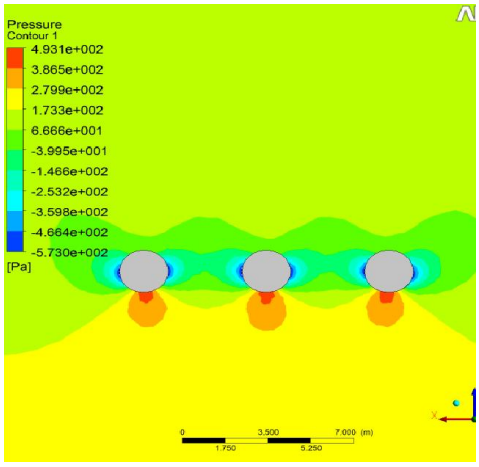

Figure 4.14b: Pressure contour with three piers

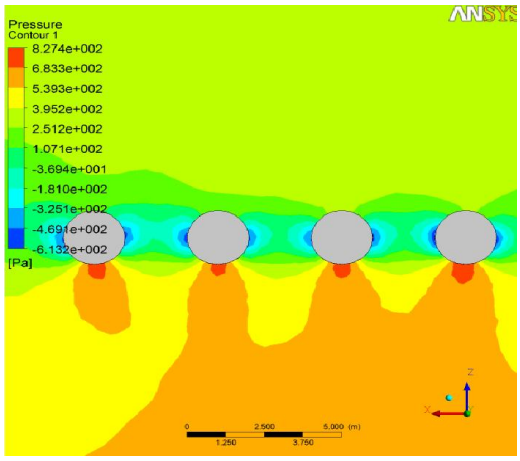

Figure 4.14c: Pressure contour with four piers

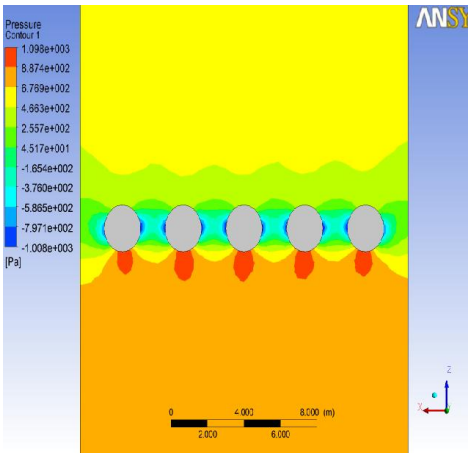

Figure 4.14d: Pressure contour with five piers

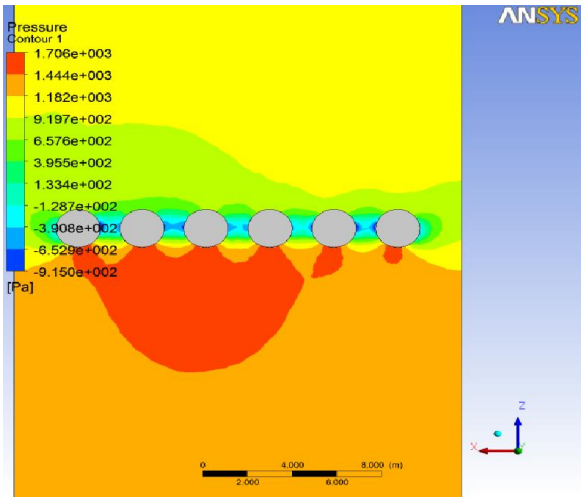

Figure 4.14e: Pressure contour with six piers

Figure 4.14: Pressure contour around multiple slender structures

It is observed from Figure 4.14 that the interference of pressure field occurs when r values less than 0.43. The pressure difference in upstream and downstream of the piers will cause more shear stress in the bed as well as in the surface of the pier.

The pressure variation at the downstream and upstream of the cylindrical barrier is presented in Figure 4.15 and 4.16 for different obstruction ratio r. The barriers are mounted on rigid bed and the pressure variation is calculated along the width of the channel section of 20m. It is observed that if the number of obstruction increases pressure variation is more. In this case at r=0.43 i.e. six number of barriers in the flow path, the pressure variation is highest and in case of two piers the pressure variation is lowest. The variation of pressure in upstream and downstream section is there. The pressure in upstream is more compared to downstream.

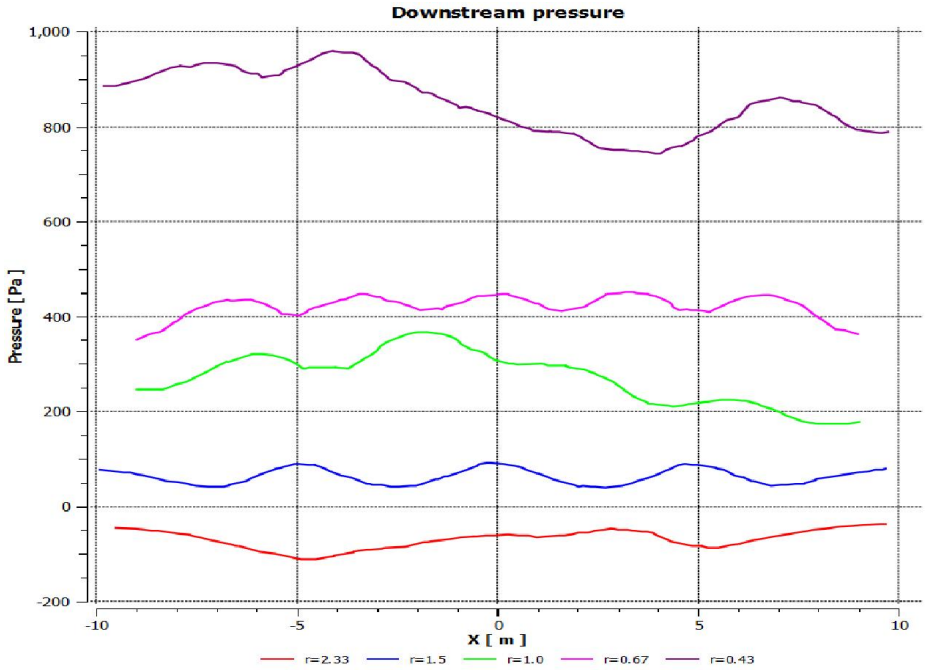

Figure 4.15: Pressure variation at 0.2m downstream of the piers line

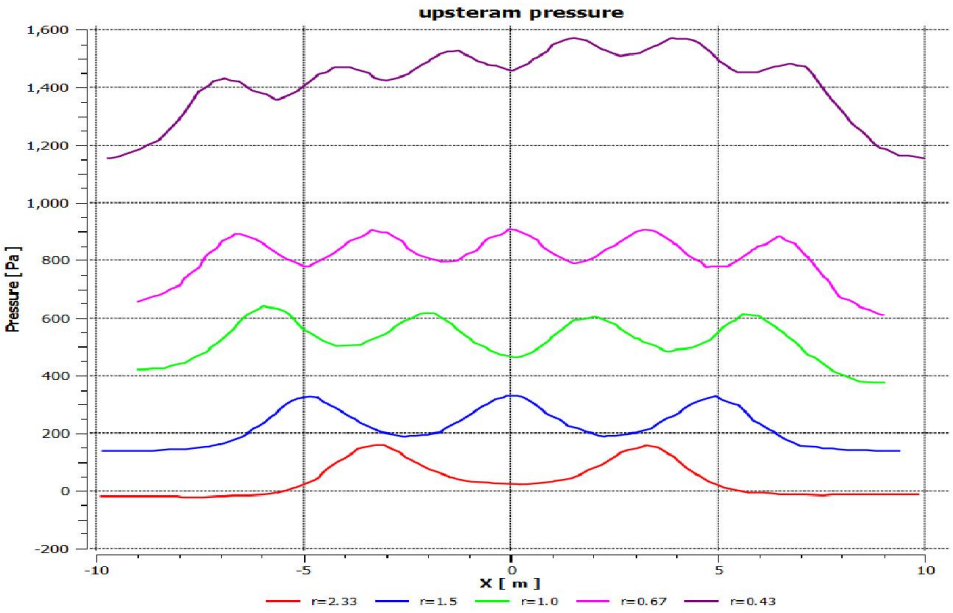

Figure 4.16: Pressure variation at 0.2m upstream of the piers line

The turbulence kinetic energy of flow changes when there is obstruction in flow path. The variation of turbulent kinetic energy for different number of pier is calculated and presented in figure 4.17

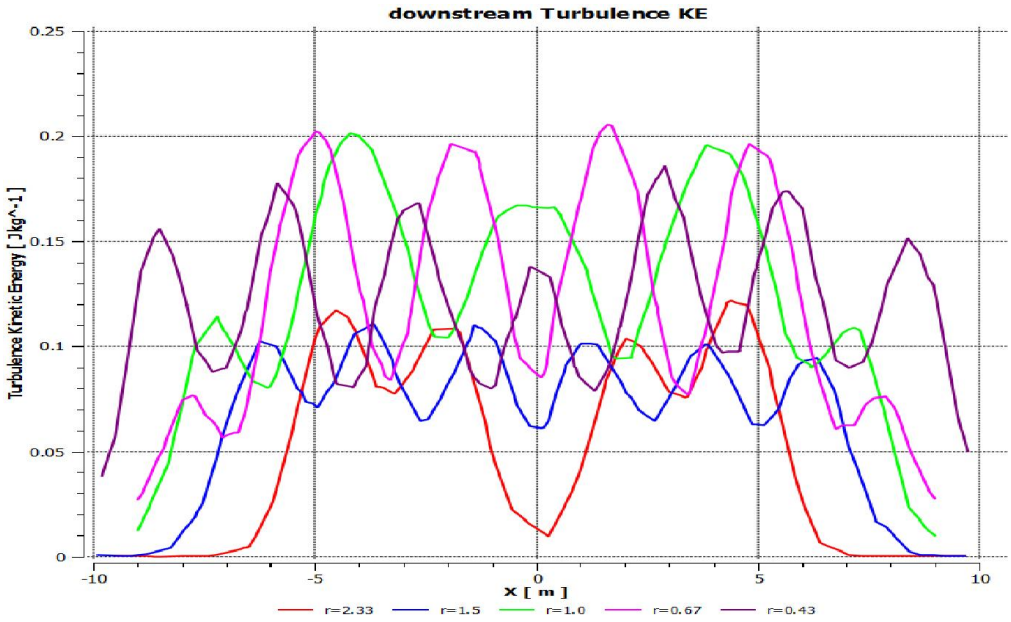

Figure 4.17: Turbulence kinetic energy

4.4 Influence of slender structure in erodible channel section

The bed of natural stream is mostly erodible in plane region. The bed is naturally constituted by different type soil, and this soil layer may be homogeneous and heterogeneous. The channel bed may be a sand layer or mixture of sand and clay layer. When the piers are mounted on this type bed the channel bed is susceptible to scour hole formed.

HEC-RAS is an integrated system of software, designed for interactive use in a multi-tasking environment. HEC-RAS is designed to perform one-dimensional hydraulic calculations for a full network of natural and constructed channels.

In this section, the scour depth around cylindrical pier is determined using HEC- RAS software. Initially, the analysis is carried out with the similar boundary conditions of present experimental study. The analysis of the same model (used in experimental study) is carried out and results are produced to check the experimental data and analysis results. It is observed from analysis that the results are quite similar.

HEC RAS analysis is carried out for a channel section of width 0.43m same as experimental study. The bottom of the model is covered with 15 cm sand stratum with d_{50} = 0.163mm and specific gravity 2.59. The water depths upstream the piers were measured by the point gauge of the flume. The depth of flow and discharge data obtained in the experimental study is used in HEC-RAS model to study the maximum sour depth around pier.

4.4.1 Scouring of channel section around cylindrical pier

The model of cylindrical pier on erodible channel bed is presented in Figure 4.18. The diameters of pier are used 2.25cm and 3.18cm and discharge is in the range 150 liter/ minute, 180 liter/minute and 200 liter/ minute. A typical 3-D view of the model is shown in Figure 4.18.

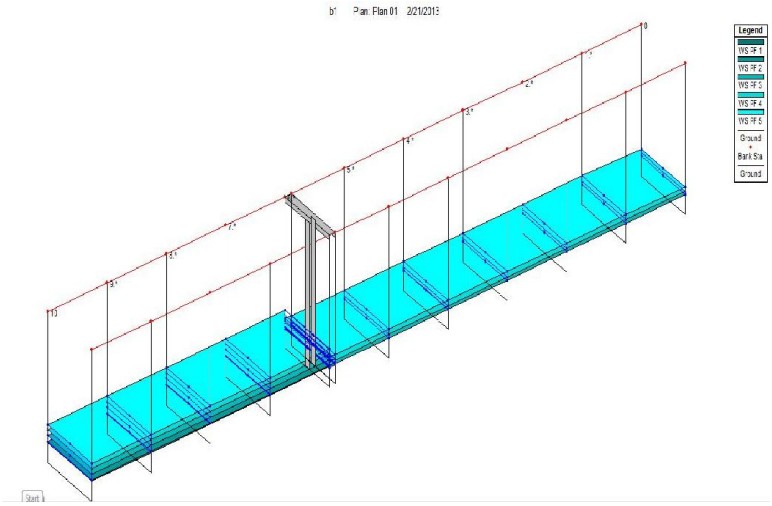

Figure 4.18: Pier embedded in sand bed in model

The different input parameters that are used in the analysis of model of a circular cylinder are presented in Table 4.1. The depths of flows in the channel section are kept in model 1.7 cm, 1.9cm and 2.1 cm above the sand bed. The CSU equation is used for calculation purpose.

Table 4.1: Input parameters

Input Parameters	Values
K1 Nose Shape	1.0
Pier Angle	0
K2 Angle Coefficient	1.0
K3 Bed Cond Coefficient	1.1
Grain Size D_{90} (mm)	0.33
Grain Size D_{50} (mm)	0.163
K4 Armouring Coefficient	1

Table 4.2: Output Parameters for pier diameter 2.25cm

Discharge (lit/min)	150	180	200
Depth of flow Upstream (m)	0.0200	0.0221	0.0239
Velocity Upstream (m/s)	0.2906	0.3157	0.3236
Froud Number	0.66	0.68	0.69
Average Bed Shera stress (N/m^2)	0.0283	0.0324	0.0332
Energy loss (m) around upstream and downstream of piers	0.00066	0.00045	0.00032

The shape of the scour hole obtained in HEC-RAS analysis is presented in Figure 4.19. It is observed that maximum scour depth is Maximum scour depth 0.038cm for a discharge 180 liter/minutes.

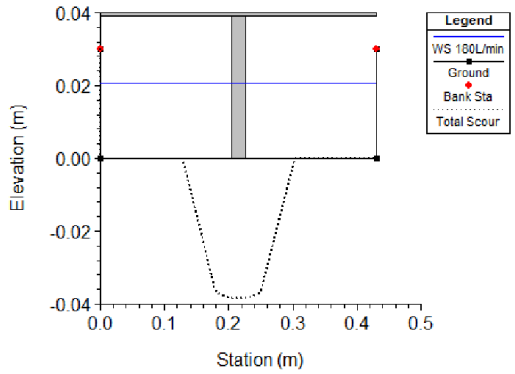

Figure 4.19: Scour depth around pier model of diameter 2.25cm

Table 4.3: Output Parameters for pier diameter 3.18cm

Discharge (lit/min)	150	180	200
Depth of flow Upstream (m)	0.0203	0.0235	0.0244
Velocity Upstream (m/s)	0.2857	0.2972	0.3177
Froud Number	0.64	0.62	0.65
Average Bed Shera stress (N/m^2)	0.0272	0.0282	0.0318
Energy loss (m) around upstream and downstream of piers	0.00011	0.00039	0.00050

The shape of the scour hole obtained in HEC-RAS analysis is presented in Figure 4.20. It is observed that maximum scour depth is Maximum scour depth 0.058cm for a discharge 150 liter/minutes.

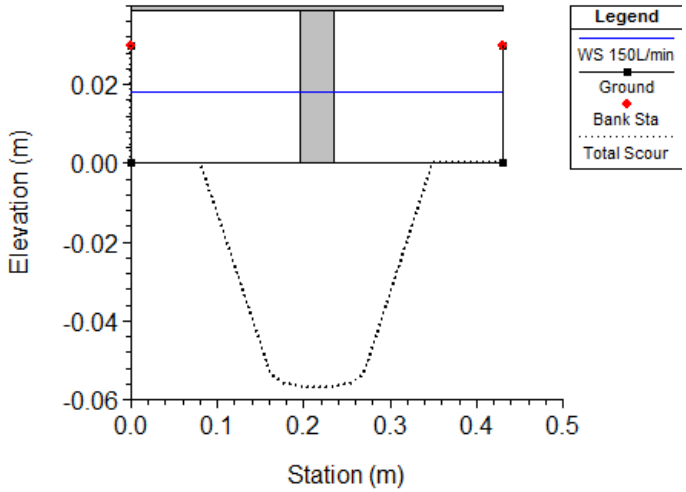

Figure 4.20: Scour hole for circular pier of diameter 3.18 cm

For rectangular pier same analysis is carried out for the input parameters and output parameters are obtained in the Table 4.4.

Table 4.4: Output Parameters for rectangular pier 3.38 x 3.04m

Discharge (lit/min)	150	180	200
Depth of flow Upstream (m)	0.0250	0.0300	0.0330
Velocity Upstream (m/s)	0.2845	0.2959	0.3078
Froud Number	0.66	0.68	0.69
Average Bed Shera stress (N/m^2)	0.0269	0.0279	0.0296
Head loss (m)	0.000186	0.000201	0.000187

Comparative study of experimental and HEC-RAS is presented in Table 4.5. It is observed from Table 4.5 that for similar boundary conditions, the HEC-RAS results are quite similar to present experimental results.

Table 4.5: Comparative result of experimental study and HEC-RAS

Discharge (liter/minute)	Circular Pier diameter (cm)				Rectangular Pier (cm x cm)			
	Experimental		HEC-RAS		Experimental		HEC-RAS	
	2.25	3.18	2.25	3.18	3.38x3.04	4.15x4.04	3.38x3.04	4.15x4.04
	Scour Depth (m)							
150	0.033	0.0429	0.039	0.058	0.049	0.0530	0.0521	0.057
180	0.037	0.0482	0.038	0.061	0.051	0.0546	0.0534	0.059
200	0.0406	0.0519	0.041	0.061	0.0567	0.0588	0.0542	0.069

4.4.2 Bed shear stress

The HEC-RAS model is used to find the bed shear stress for the model. The variation of bed scour depth for non-dimensional quantity h/B=0.4 and d/B=0.1 is calculated as the same boundary conditions. The variation of scour depth with discharge is presented in Figure 4.21. It is observed that as the discharge is increasing the maximum scour depth increases as per CSU equation.

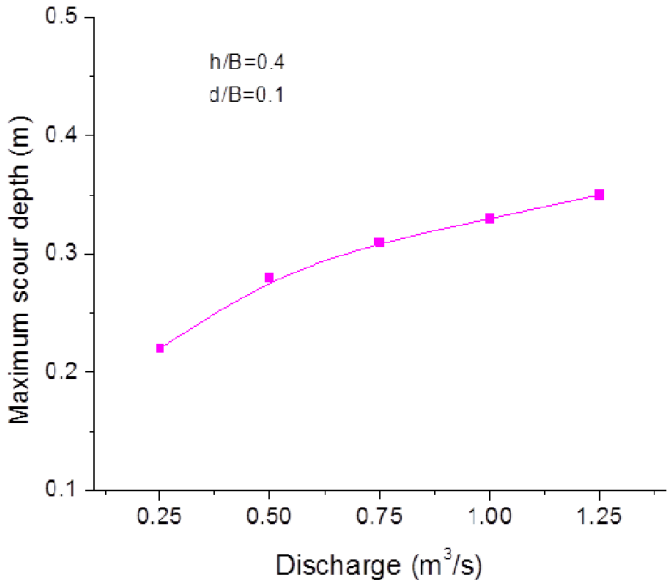

Figure 4.21: Maximum scour depth with discharge

The bed shear stress changes with velocity of flow. The bed shear stress variation for a different mean velocity is presented in Figure 4.22.

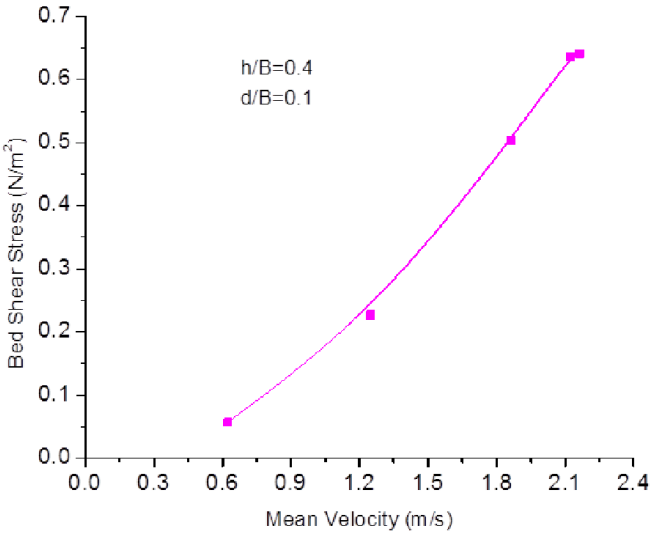

Figure 4.22: Maximum bed shear stress with mean velocity

4.5 Bed Shear stresses and pier shear stress

The bed shear stress and shear stress on pier are found in rigid rectangular and trapezoidal channel section. The effect of characteristic diameter of slender structure and channel geometry on shear stresses are analyzed using ANSYS v14.0 FLUENT. Volume of Fluid (VOF) and k-epsilon turbulence model were used for the simulation setup. Prior to the setup of simulation, discretization of 3D model of channel was done. The resultant discretization of the model had sufficient nodes to minimize errors. Proper boundary conditions were imposed for different sections of the model. Zero roughness height and no slip wall conditions i.e. fluid will have zero velocity with respect to boundary, were imposed on pier, bed and wall of channel. Finally proper number of iterations was employed. The k-ϵ model constant are used as follows: $c_{\mu} = 0.09$, $c_{1\varepsilon} = 1.44$, $c_{2\varepsilon} = 1.92$, $\sigma_k = 1$ and $\sigma_{\varepsilon} = 1.3$.

The geometry of the rectangular and S-shape channel section with cylindrical pier is shown in Figure 4.23. The depth of flow is h, channel width B and diameter of circular pier is d.

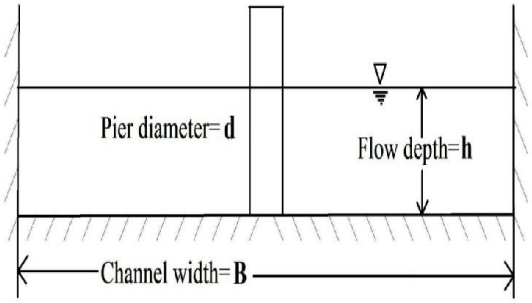

Figure 4.23(a): Rectangular channel cross section with pier at the middle of the channel

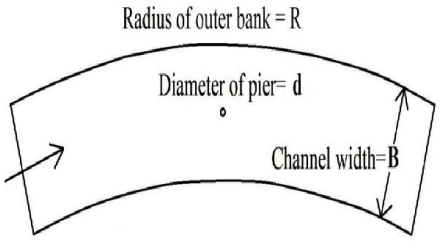

Figure 4.23(b): S-shaped channel cross section with pier at the middle of the channel

For validation purpose of the numerical model, initially a rectangular channel section having width 30m and depth of flow 5m is considered without any obstruction in the channel section. Bed shear stress at mid of rectangular channel section is found and plotted against mean flow velocity in Figure 4.24. Quadratic relationship is observed between bed shear stress and mean velocity which is in accordance with quadratic stress law.

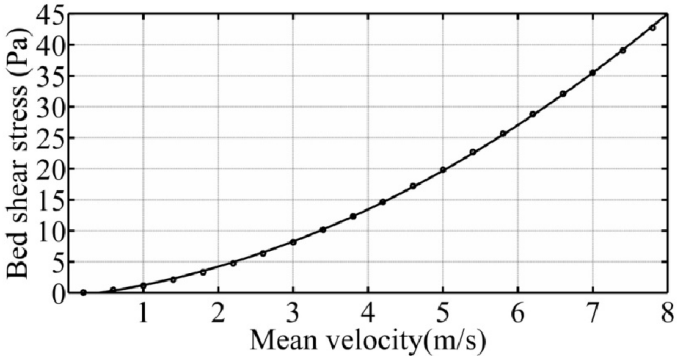

Figure 4.24: Bed shear stress at mid of rectangular channel with mean velocity of flow

The bed shear stress is found for rectangular channel section for different channel width keeping depth of flow constant. The variation of maximum bed shear at the bottom of

the pier section and maximum shear stress at the surface of the pier is computed and presented in Figure 4.25 and 4.26.

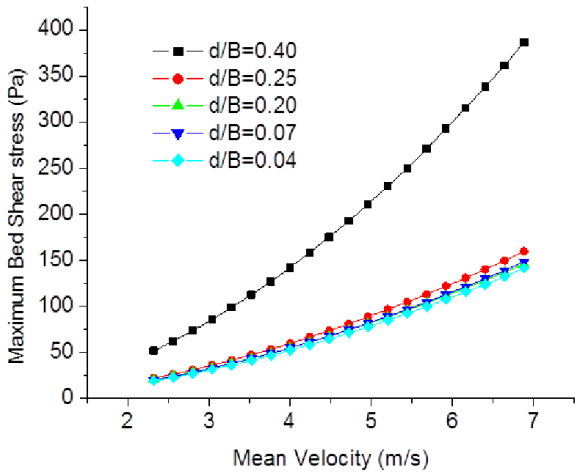

Figure 4.25: Maximum bed shear stress variation with mean flow velocity for rectangular channel section

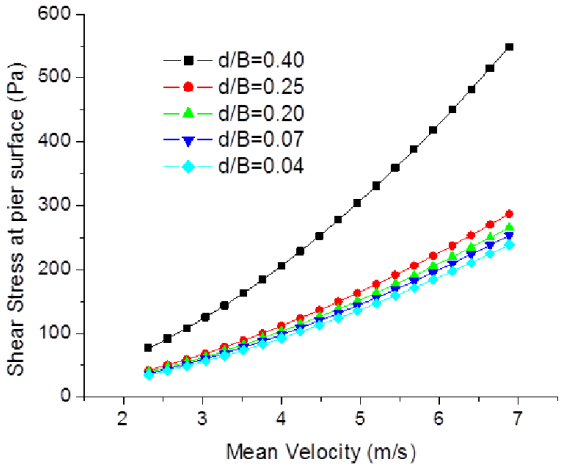

Figure 4.26: Maximum shear stress variation at pier surface with mean flow velocity in rectangular channel section

It is observed from Figure 4.25 that for low flow velocities, the maximum bed shear stress comes almost same for large channel aspect ratio (i.e. ratio of channel width and depth of flow) of the channels. In case of high flow velocities, bed shear stress decreases with increase in channel aspect ratio. In case of high flow velocities, bed shear stress

decreases with increase in channel aspect ratio. Similar variation pier shear stress observed in Figure 4.26.

The variation of maximum bed shear stress and maximum shear stress at the surface of the pier is computed and presented in the Figure 4.27 and 4.28 for different channel section. In case of rectangular shaped channel and s-shaped channel having large channel aspect ratios and low flow velocities it is observed that the shape of channel does not have any effect on maximum shear stress in bed shear and pier shear. It was observed that for low flow velocities and large channel aspect ratios, the maximum shear stress in bed and pier remains unchanged for rectangular and s-shape channel cross sections.

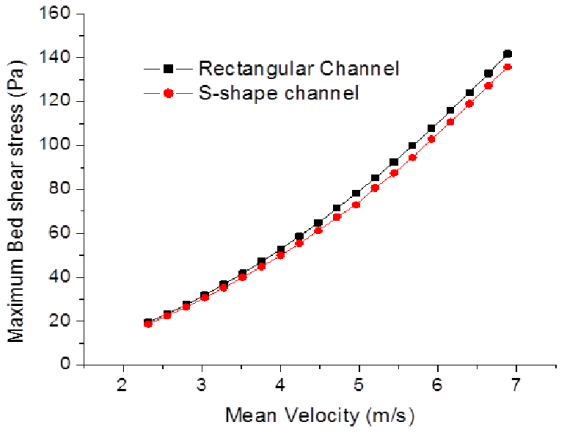

Figure 4.27: Maximum bed shear stress variation with mean velocity

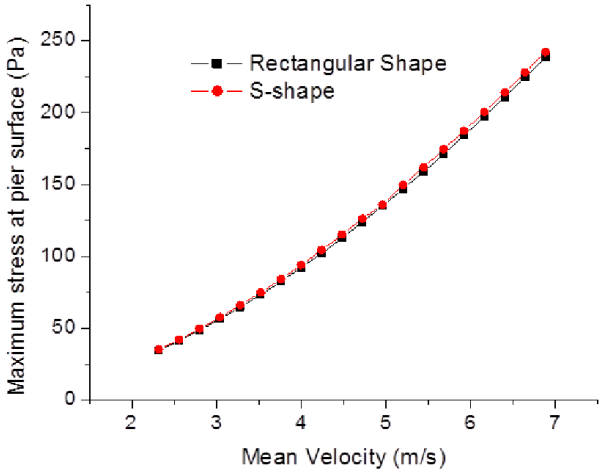

Figure 4.28: Maximum pier shear stress variation with mean velocity